Research on The Structural Integrity of HTGR Reactor Pressure Vessels by Using Probabilistic Fracture Mechanics

Bowen Li[a*], Haitao Wang[a]
[a]Institute of Nuclear and New Energy Technology of Tsinghua University, Collaborative Innovation Center of Advanced Nuclear Energy Technology of Ministry of Education, Key Laboratory of Advanced Reactor Engineering and Safety of Ministry of Education, Beijing, China

Abstract: Probabilistic fracture mechanics has been widely applied to evaluate the structural integrity of reactor pressure vessels (RPVs) under various transient conditions from a probabilistic perspective. Based on probabilistic fracture mechanics, this paper focuses on the failure probability of the RPV of a pebble-bed modular HTGR (HTGR-RPV) under a typical transient condition. The geometrical characteristics, fast-neutron irradiation conditions, transient temperature of inner and outer walls of the HTGR-RPV and the hypothesis of its flaw distributions are given. In addition, the influence of several different flaw sizes on the failure probability is investigated in consideration of the potential adjustment of manufacturing specifications for the HTGR-RPV in the future which might lead to differences of related flaw information. The results indicate that even under conservative assumptions of flaw sizes, the failure probability of the HTGR-RPV is extremely low, which attributed to the low fast neutron levels and slow transient development.

Keywords: High Temperature Gas-cooled Reactor, Probabilistic Fracture Mechanics, Reactor Pressure Vessel, Structural Integrity Evaluation.

1. INTRODUCTION

Structural integrity of the RPV is essential to the reactor safety. In the design phase of the RPV, factors considered in the structural analysis, such as dispersion of the material, the changes in material properties caused by environmental factors during service, the randomness of the flaws of components, and the varying degrees of randomness of external loads, the stress levels and strength at dangerous points, has to be properly addressed[1][2]. In this paper, structural integrity of the RPV of a pebble-bed modular HTGR is studied by using the probabilistic fracture mechanics. The RPV core belt region under irradiation conditions is analyzed with considering specific RPV geometric dimensions, material properties, fast-neutron fluence, typical transient, flaw distributions and other parameters of the HTGR. The failure frequency of the RPV is calculated accordingly. Considering importance of the safety function of a HTGR-RPV in terms of containing the primary coolant is different from that of a PWR, it might be feasible for the HTGR-RPV to adopt the design and manufacturing rules other than Safety Class 1 related rules (Subsection NB of ASME BPVC Section III, Div 1 as an example) in the future, which introduces the potential differences in manufacturing-induced flaws. Therefore, several types of flaw distribution sizes are compared and analyzed in this paper.

2. PARAMETERS OF A PEBBLE-BED MODULAR HTGR

2.1. The Reactor Pressure Vessel

This paper focuses on a 290MWth pebble-bed modular HTGR. The probabilistic fracture mechanics analysis model for the core belt region of the HTGR-RPV is established. The HTGR-RPV does not have an inner cladding layer, which is different from the PWR. The core belt region is of a cylinder shape with an inner diameter of 5700mm and a wall thickness of 141mm, which is thinner than the thickness of a typical PWR. The total height of the core belt region is 11000mm, with four circumferential welds and no axial welds. The height of the circumferential welds is assumed to be 25mm, and the cylinder is divided into five cylinder sections by the circumferential welds. Therefore, the entire core region is divided into nine main parts as shown in Figure 1, and each part is further subdivided into several circumferential subregions.

2.2. Irradiation Embrittlement Model and Material Parameters

The irradiation-induced shift of reference nil-ductility transition temperature, ΔRT_{NDT}, is calculated by using the radiation embrittlement prediction model from R.G 1.99 Rev.2[3]. The base material of the HTGR-RPV is

SA-508-3-1 steel forgings, which is the same as PWRs. Considering the randomness of the material composition, the best estimate of Cu content is assumed to be 0.1%, and the best estimate of Ni content is assumed to be 0.8% for the base material. The best estimate of Cu content is assumed to be 0.05% and the best estimate of Ni content is assumed to be 0.8% for the welds[4]. For both the base material and the welds, the best estimated value of non-irradiated reference nil-ductility transition temperature RT_{NDT0} is not higher than -20°C. This paper conservatively sets RT_{NDT0} as -20°C. The material of the HTGR-RPV meets the requirements of RG1.99 Rev.2, while the main difference is that its irradiation temperature (~200°C) is lower than the standard-specified temperature. Therefore, based on the RG1.99 Rev.2 formula, a temperature correction value, $RT_{NDT-cor}$, is added to establish the irradiation prediction model for the HTGR-RPV. The temperature correction value is taken as 30°C, which can encompass the measured RT_{NDT} (maximum 24.6°C) of the material at irradiation temperatures ranging from 60°C to 288°C[5][6]. The standard deviation of RT_{NDT0} is 0 for base material and 17°F for weld[7]. The Cu content, Ni content, and RT_{NDT0} are sampled according to their normal distribution within each subregion, which represented the uncertainty of the material distribution along the axial direction of the RPV.

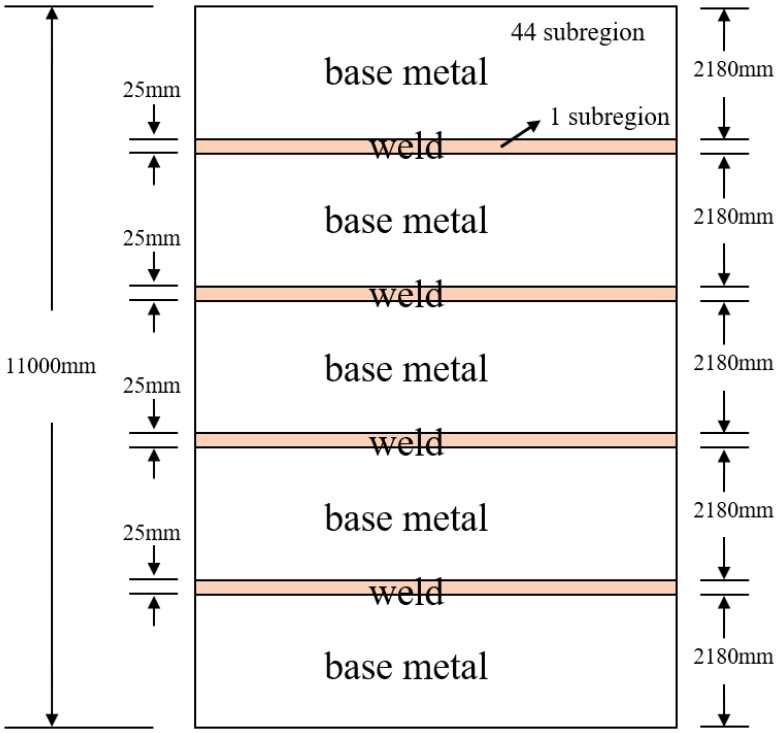

Figure 1. The Reactor Pressure Vessel Model

2.3. Fast-neutron Fluence

The fast-neutron fluence of the 290MWth pebble-bed modular HTGR in this paper is roughly estimated by scaling-up of the fast-neutron fluence of the 250MWth HTR-PM demonstration plant. Considering the core position, the fast-neutron fluence distribution shape along the axial direction of the inner wall of the HTGR-RPV is shown in Figure 2. The peak value of the accumulated fast-neutron fluence at the end of 60 years of service life is ~5.5E17n/cm2.

2.4. Transient Parameter

Loss of feed water in the secondary loop is one of the typical transients assumed for the HTGR, and its frequency is assumed to be ~2E-01 times/reactor-year. During this transient, the temperatures of both the inner and outer wall surfaces of the RPV firstly decrease and then grow, and the pressure inside the RPV rapidly increases and decreases briefly, then rises again and eventually stabilizing at a value higher than the initial pressure. In this paper, with the Loss of feed water in the secondary loop as a typical transient, the worst conditions of internal and external wall temperatures and the internal wall pressure are assumed uniformly distributed along the height direction, as shown in Figure 3. With referring to Appendix E of ASME Section XI[8] and making appropriate modifications, a residual stress which is +69MPa at both the internal and external

surfaces of the vessel and linearly distributes along the vessel wall is assumed as shown in Figure 4. Taking Figure 3 as the boundary conditions, the temperature field and stress field along the wall thickness are calculated.

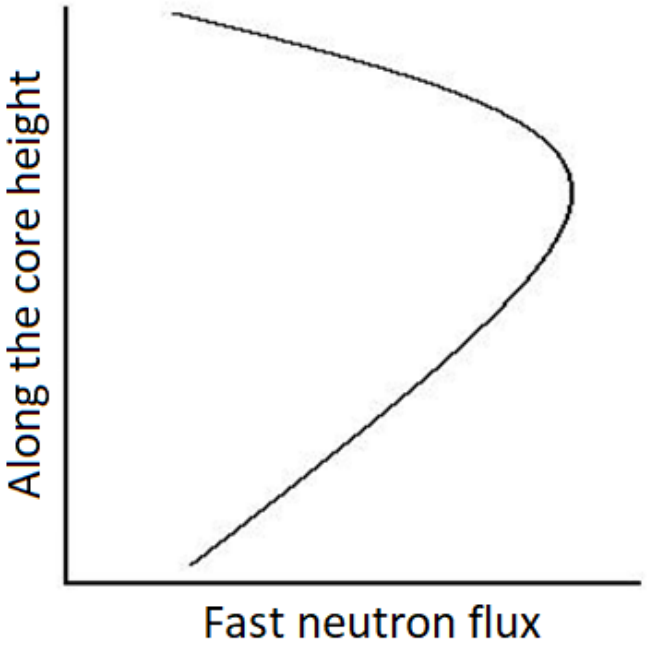

Figure 2: Fast-neutron Flux Distribution on the Inner Wall of the HTGR-RPV

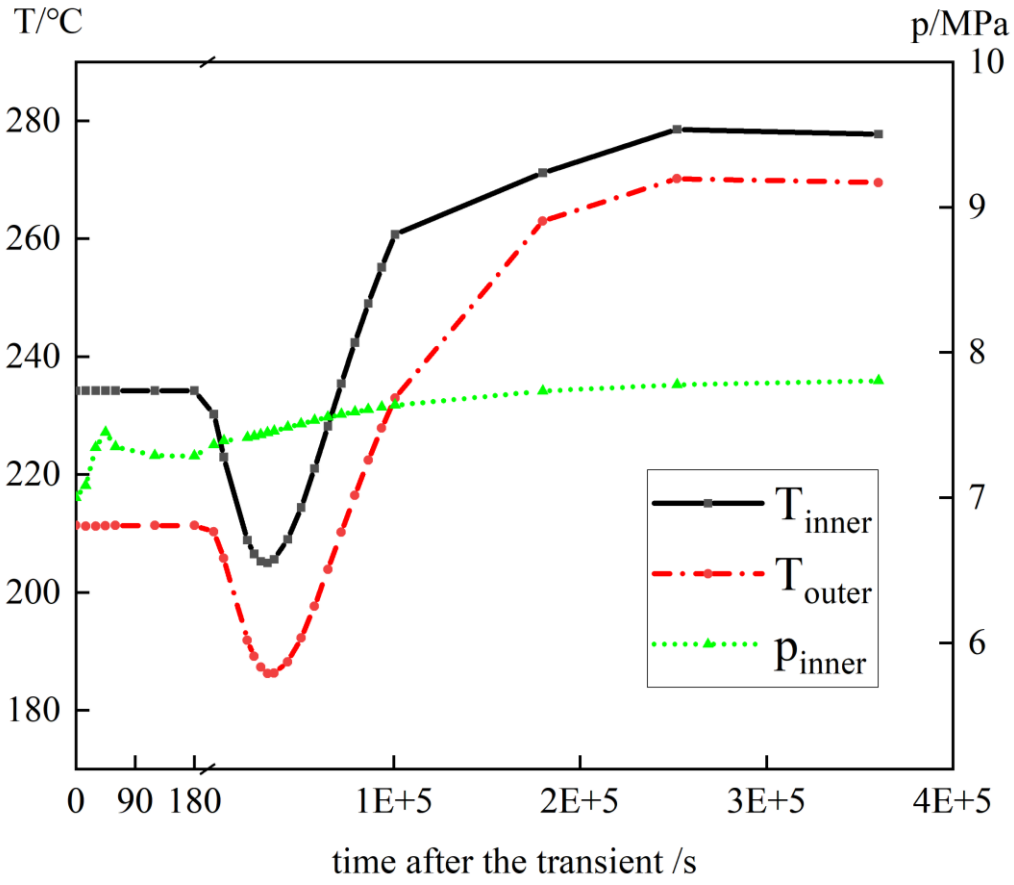

Figure 3: Boundary Conditions of the Vessel Wall during the Loss of Feed Water in the Secondary Loop Transient

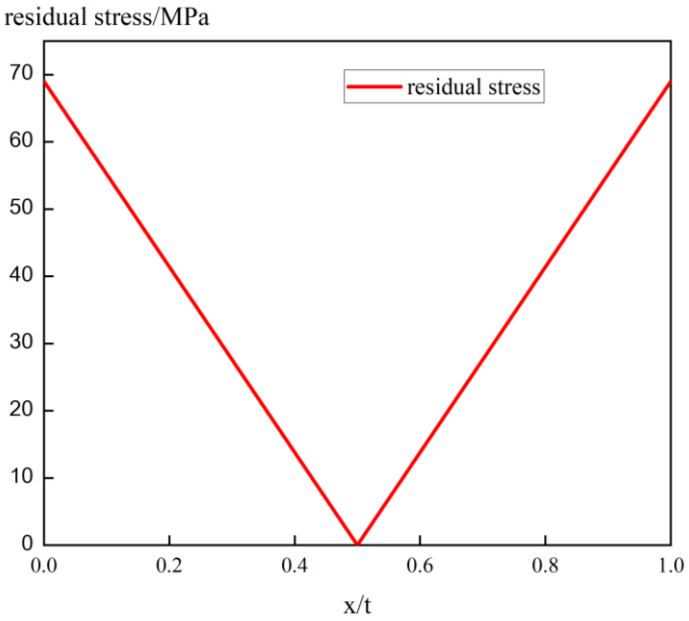

Figure 4: Residual Stress Distribution along the wall thickness

3. ANALYSIS AND CALCULATION METHODS

3.1. Flaw Distribution and Stress Intensity Factor Calculation

With the calculated stress field distributed along the wall thickness, type I stress intensity factor (K_I) of several types of flaws can be calculated such as semi-elliptical finite surface flaws (axial and Circumferential), infinite axial surface finite flaws, 360° continuous circumferential surface flaws, and elliptical finite subsurface flaws (axial and Circumferential) according to Appendix A of ASME Section XI[8].
The distribution of flaw depth (***a*** for surface flaw, ***2a*** for subsurface flaw) and aspect ratio (***a/L*** for surface flaw, ***2a/L*** for subsurface flaw) is given by reference[9]. Surface flaws which are evenly divided between the inner and outer walls and subsurface flaws located over the entire thickness range of the vessel wall are considered[10]. For subsurface flaws, the flaw location ***d*** is uniformly distributed along the thickness. Subsurface flaws and surface flaws are shown in Figure 5.

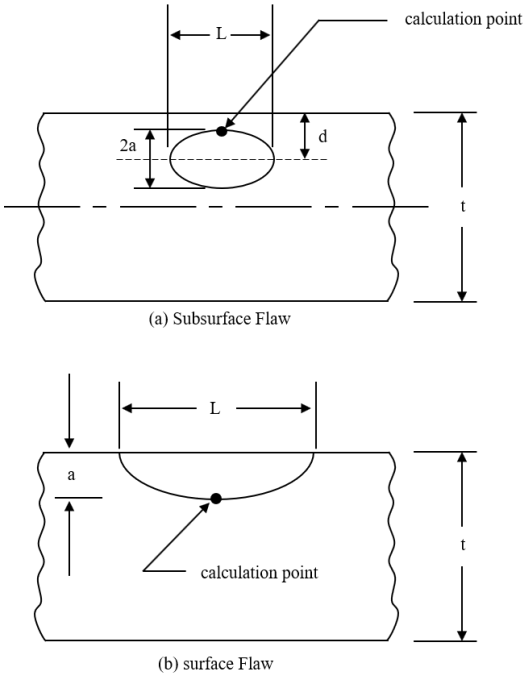

Figure 5: Elliptical and Semi-elliptical Flaw Models[8]

3.2. Probabilistic Fracture Mechanics Analysis and Calculation

The calculation process of probabilistic fracture mechanics is shown in the Figure 6. Main steps are as follows.
Step 1: RPVs with the flaw distribution mentioned in section 3.1 are constructed, and the number of flaws is sampled according to the distribution in each pressure vessel ***j***. The epistemic uncertainty of RT_{NDT}, $RT_{epistemic}$, is sampled in each RPV according to the following Weibull distribution. For each subregion of the RPV, Cu content, Ni content, RT_{NDT0}, and fast-neutron fluence of the inner wall are sampled[7].

$$\Delta RT_{epistemic} \leftarrow W(-34.167, 43.333, 1.73)$$
$$\Delta RT_{epistemic} = -34.167 + 43.333[-\ln(1-\Phi)]^{1/1.73} \quad [°C]$$
$$\Phi \leftarrow U(0,1)$$

Step 2: For each flaw ***k***, the flaw location ***d*** (only for subsurface flaw) is sampled. Then ΔRT_{NDT} is calculated, and RT_{NDT} is calculated according to the following formula[7]. Its aspect ratio (***a/L*** for surface flaw, ***2a/L*** for subsurface flaw) is sampled accordingly.

$$RT_{NDT} = RT_{NDT0} - \Delta RT_{epistemic} + \Delta RT_{NDT}$$

Step 3: At each time step ***n***, the parameter $a_{K_{Ic}}$, $b_{K_{Ic}}$,$c_{K_{Ic}}$ of the weibull distribution of the static cleavage fracture initiation toughness (K_{Ic}) of the flaw is calculated. K_I is calculated according to the stress field, and its conditional probability of crack initiation $cpi_{j,k,n}$ is obtained according to the weibull distribution[7]

$$a_{K_{Ic}} = 672.3831 + 289.6286\exp[0.02254(\Delta T_{RELATIVE})] \quad \text{MPa}\cdot\sqrt{\text{mm}}$$
$$b_{K_{Ic}} = 542.4238 + 1742.0109\exp[0.008(\Delta T_{RELATIVE})] \quad \text{MPa}\cdot\sqrt{\text{mm}}$$
$$c_{K_{Ic}} = 4$$
$$cpi_{j,k,n} = 1 - \exp\left[-\left(\frac{K_I - a_{K_{Ic}}}{b_{K_{Ic}}}\right)^{c_{K_{Ic}}}\right]$$

Where $\Delta T_{RELATIVE} = T - RT_{NDT}$ in °F.
Step 4: The maximum $cpi_{j,k,n}$ in each time step is taken as the conditional probability of crack initiation $CPI_{j,k}$ of flaw ***k***, and the crack arrest probability is calculated in the crack arrest subprocess.
Step 5: Calculate the probability that at least one crack initiates in RPV ***j*** as the initiation probability CPI_j of RPV ***j***, and calculate the probability that at least one crack fails in RPV ***j*** as the failure probability CPF_j of RPV ***j***.
Step 6: The conditional initiation probability CPI of the transient is calculated by averaging the failure probability CPI_j of all RPVs. The conditional failure probability CPF of the transient is calculated by averaging the failure probability CPF_j of all RPVs.
Step 7: The crack initiation frequency Φ_I and failure frequency Φ_F of the transient are calculated.

3.3. Subprocess - Crack Arrest Calculation Process

Consider crack propagation as a step-by-step process, calculating at the end of each propagation step whether the crack can arrest. If it arrests, assess whether the crack re-intiates. If it re-intiates, repeat the step-by-step propagation process mentioned above. The crack fails if crack extend to a certain depth before the transient ends. If the crack does not extend to the certain depth by the end of the transient, it is considered as a stable crack arrest.
Arrest-step 1: For each time step with an increasing crack initiation probability ($dcpi_{j,k,n}/dt>0$?), it is considered to have crack growth potential and several crack arrest tests are performed.
Arrest-step 2: Each crack with propagation potential expands into an infinite axial or 360° continuous circumferential surface cracks[7][11] at the next time step after initiation.
Arrest-step 3: The crack arrest toughness (K_{Ia}) with a lognormal distribution is calculated to determine whether the crack arrest.
Arrest-step 4: If the crack arrests, advance the time step forward and recalculate at each time step whether it re-intiates.
Arrest-step 5: If the crack does not arrest or the crack re-intiates, advance the crack depth forward and calculate whether the crack is arrest at each depth mesh.

Arrest-step 6: If the time step successfully reaches the end of the transient state, the crack successfully arrests. And the crack fails if the crack depth reaches the specified limit on crack depth or the remaining wall thickness of the RPV cannot provide the stress required to maintain the RPV integrity.
Arrest-step 7: From the crack's initiation time step to the time step with the maximum $cpi_{j,k,n}$, the conditional probability of crack failure $CPF_{j,k}$ of the flaw ***k*** is calculated.

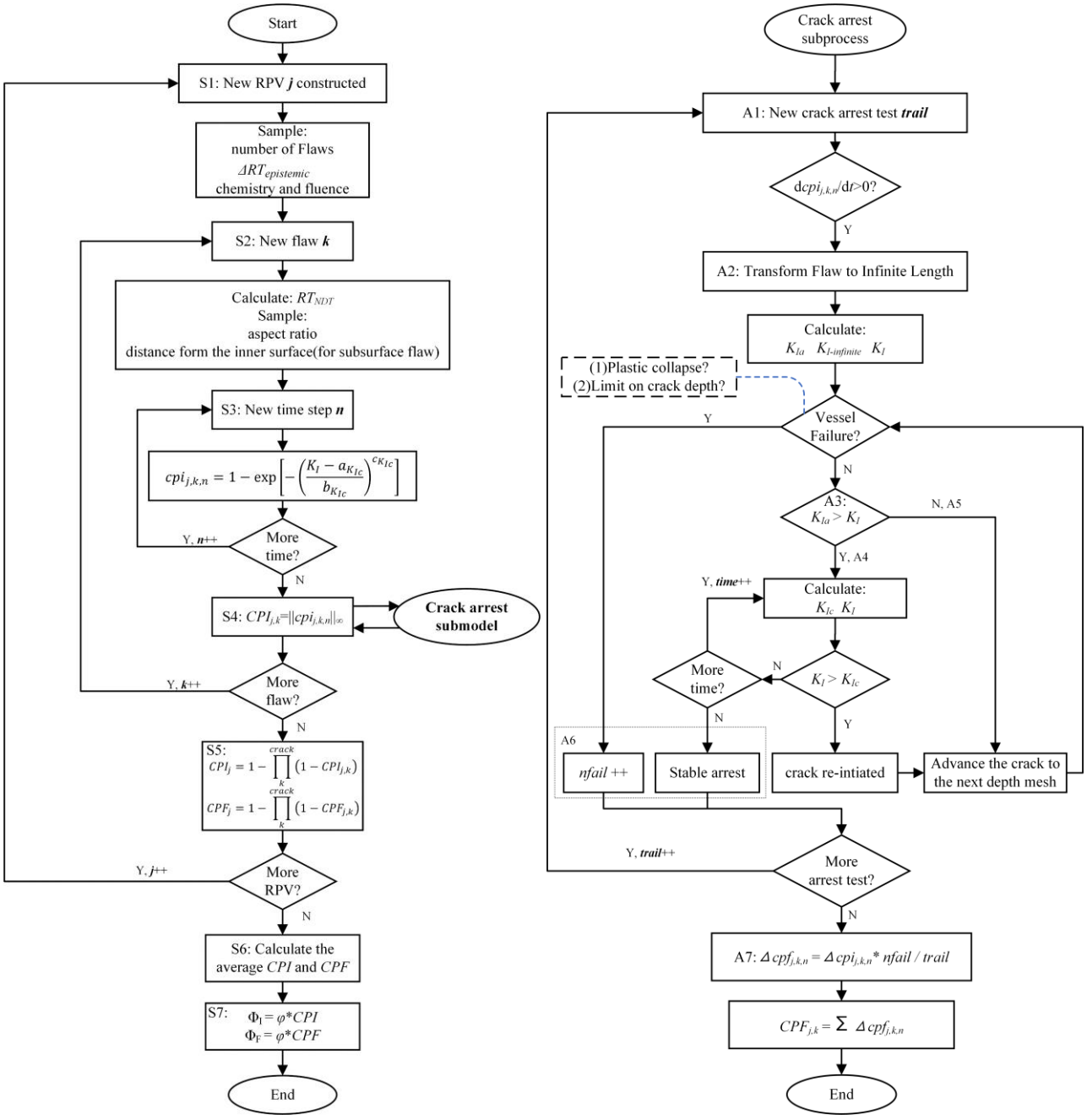

Figure 6: Calculation Process of Probabilistic Fracture Mechanics

4. RESULTS AND DISCUSSION

In order to simulate possibly more severe flaw conditions due to differences in manufacturing specifications and to obtain the safety margin of the depth and density of flaws, during the calculation process, the aspect ratio of flaws is kept constant, and the depth and density of flaws are amplified by a certain factor. There are three examples performed:
(1). The flaw depth and density are amplified by 1 times (original value).
(2). The flaw depth and density are amplified by 2 times.
(3). The flaw depth and density are amplified by 4 times.

The calculated results of CPI and CPF are shown in Table 1. When the flaw depth and density are amplified by 1, 2 and 4 times, both the CPI and CPF are 0. The reasons might be:
(1). The transient developed slowly, resulting in relatively low stress levels along the RPV wall thickness and a small K_I accordingly.
(2). The transient temperature is not extremely low and the level of fast-neutron fluence is low, which leads to a high $\Delta T_{RELATIVE}$, thus K_{Ic} is high.

Table 1: Results of CPI and CPF when the Temperature Correction is 30℃

	Flaw depth and density ×1	Flaw depth and density ×2	Flaw depth and density ×4
CPI	0.00E+00	0.00E+00	0.00E+00
CPF	0.00E+00	0.00E+00	0.00E+00

In order to obtain the non-zero value and get the comparison of the safety margin of the vessel under different flaw distributions, the temperature correction is increased from 30℃ to 130℃ and 230℃ (it is actually impossible in practice, and it is only to make a comparison of non-zero results mathematically) while keeping other parameters constant. Table 2 shows the calculation results of CPI and CPF when the temperature correction value is 130℃ and 230℃, respectively. It is shown that when the temperature correction value is assumed 130℃, both the CPI and CPF are still 0. Only when the temperature correction value is assumed 230℃, the CPI and CPF will have non-zero values. In this temperature correction condition, both the CPI and CPF will increase by several orders of magnitude when the flaw depth and density are amplified by 2 and 4 times.

Table 2: Results of CPI and CPF when the Temperature Correction is 130℃ and 230℃

		Flaw depth and density ×1	Flaw depth and density ×2	Flaw depth and density ×4
$RT_{NDT\text{-}cor}$ =130℃	CPI	0.00E+00	0.00E+00	0.00E+00
	CPF	0.00E+00	0.00E+00	0.00E+00
$RT_{NDT\text{-}cor}$ =230℃	CPI	1.86E-07	3.63E-04	9.46E-02
	CPF	1.86E-07	3.63E-04	9.44E-02

Results of crack initiation frequency Φ_I and failure frequency Φ_F of the transient are shown in Table 3.

Table 3: Results of Φ_I and Φ_F

		Flaw depth and density ×1	Flaw depth and density ×2	Flaw depth and density ×4
$RT_{NDT\text{-}cor}$ =30℃	Φ_I	0.00E+00	0.00E+00	0.00E+00
	Φ_F	0.00E+00	0.00E+00	0.00E+00
$RT_{NDT\text{-}cor}$ =130℃	Φ_I	0.00E+00	0.00E+00	0.00E+00
	Φ_F	0.00E+00	0.00E+00	0.00E+00
$RT_{NDT\text{-}cor}$ =230℃	Φ_I	4.02E-08	7.78E-05	2.04E-02
	Φ_F	4.02E-08	7.78E-05	2.04E-02

5. CONCLUSION

(1). The calculated CPI and CPF of the HTGR-RPV is zero under the condition of loss of feed water in the second loop. The results may be attributed to the very low fast neutron flux level (one to two orders of magnitude lower than a typical PWR) and slow development of the temperature transient.
(2). Considering the more conservative flaws, even if the RPV has a worse flaw conditions with the density and depth of flaws amplified by 2 times and 4 times, both the CPI and CPF are still zero, indicating a potential for the HTGR-RPV to adopt Non-Safety Class 1 related design and manufacturing rules in the future.
(3). To obtain the non-zero value of crack initiation and failure probability, RT_{NDT} is amplified to an extreme value which is practically impossible, and in this condition a non-zero value has finally been obtained, indicating a level of sensitivity of both the CPI and CPF to the flaw conditions.

Acknowledgements
This work has been supported by the academic discipline construction funds of Tsinghua University.

References

[1]. Koichi Masaki, Jinya Katsuyama, Kunio Onizawa. Probabilistic Structural Integrity Analysis of Reactor Pressure Vessels During Pressurized Thermal Shock Events. ASME. J. Pressure Vessel Technol, 136(1), 011208, 2014.

[2]. Rongshan Wang, Mingya Chen, Feng Lu, et al. The probabilistic structural integrity assessment of reactor pressure vessels under pressurized thermal shock loading. Journal of Mechanical Strength, 38(4), 838-843, 2016.

[3]. REGULATORY GUIDE 1.99-Radiation Embrittlement of Reactor Vessel Materials. U.S.NRC, Revision 2, 1988.

[4]. Boiler and Pressure Vessel Code, Section II, Ferrous Material Specifications. ASME, 2021 Edition, 2021.

[5]. F. M. Haggag. Effects of Irradiation Temperature on Embrittlement of Nuclear Pressure Vessel Steels. Effects of Radiation on Materials: 16th International Symposium, ASTM STP 1175, 1993.

[6]. Jiahua Liu, Lei Wang, Yang Liu, Xiu Song, Jiong Luo & Dan Yuan. Fracture toughness and fracture behavior of SA508-III steel at different temperatures. International Journal of Minerals, Metallurgy, and Materials, 21, 1187-1195, 2014.

[7]. P T Williams, T L Dickson, B R Bass, H B Klasky. Fracture Analysis of Vessels – Oak Ridge FAVOR, v16.1, Computer Code: Theory and Implementation of Algorithms, Methods, and Correlations. Oak Ridge National Laboratory, 2016.

[8]. Boiler and Pressure Vessel Code, Section XI, Rules for Inspection and Testing of Components of Light-Water-Cooled Plants. ASME, 2021 Edition, 2021.

[9]. F. A. Simonen, S. R. Doctor, G. J. Schuster, and P. G. Heasler. A Generalized Procedure for Generating Flaw-Related Inputs for the FAVOR Code. Pacific Northwest National Laboratory, 2003.

[10]. F A Simonen. The impact of NDE unreliability on pressure vessel fracture predictions. Journal of Pressure Vessel Technology, 107(1), 18-24, 1985.

[11]. Kunio Onizawa, Katsuyuki Shibata, Masahide Suzuki, Daisuke Kate, Yinsheng Li. Embedded Crack Treatments and Fracture Toughness Evaluation Methods in Probabilistic Fracture Mechanics Analysis Code for the PTS Analysis of RPV. ASME/JSME 2004 Pressure Vessels and Piping Conference, 2004.